Applied Catalysis B: Environmental 268 (2020) 118421

Contents lists available at ScienceDirect

Applied Catalysis B: Environmental

journal homepage: www.elsevier.com/locate/apcatb

# Oxidative coupling of a mixture of bio-alcohols to produce a more sustainable acrolein: An in depth look in the mechanism implying aldehydes co-adsorption and acid/base sites

Vincent Folliard[a], Georgeta Postole[a], Jean-François Devaux[b], Jean-Luc Dubois[c], Livia Marra[d], Aline Auroux[a,*]

[a] Univ Lyon, Université Claude Bernard Lyon1, CNRS, IRCELYON, 2 avenue Albert Einstein, 69626 Villeurbanne Cedex, France
[b] ARKEMA Centre de Recherches Rhône-Alpes (CRRA), 69493 Pierre Bénite, Cedex, France
[c] ARKEMA Direction Recherche & Développement, 420 Rue d'Estienne d'Orves, 92705 Colombes, France
[d] BAIKOWSKI, 1046 Route de Chaumontet, 74330 Poisy, France

ARTICLE INFO

*Keywords:*
Alcohols oxidative coupling
Aldehydes co-adsorption
Adsorption calorimetry
Acid/base properties
Acrolein production

ABSTRACT

The industrial synthesis of acrolein is mainly performed by propylene oxidation over bismuth-iron-molybdate catalysts. Among cleaner alternatives to produce acrolein, oxidative coupling of methanol and ethanol represents a promising way. In this work, the reaction has been performed in two separate reactors (for oxidation and aldolization) to study the role of the acid/base properties but also the competition of aldehydes adsorption over environmentally friendly spinel catalysts with various Al/Mg ratios. The acid/base properties of catalysts were investigated by $NH_3$ and $SO_2$ adsorption microcalorimetry. Further adsorption microcalorimetry studies were performed with methanol, formaldehyde, acetaldehyde and propionaldehyde to investigate the bounding properties of the reactants. The acid/base properties were correlated with acrolein yield and selectivity under oxidizing conditions. Co-adsorption of aldehydes was also investigated allowing justification of the absence of crotonaldehyde formation.

## 1. Introduction

Acrolein, with its conjugated vinyl and carbonyl groups, is a widely used intermediate molecule for numerous syntheses of high added-value industrial products such as acrylic resins, super absorbent polymers, detergents and also for feed applications, such as methionine, or biocides [1–4]. The first commercial process developed by Degussa in 1942 for the acrolein production was an aldol condensation of acetaldehyde and formaldehyde. Nowadays, the industrial synthesis of acrolein is essentially done by propylene oxidation over bismuth-iron-molybdate catalysts [4].

The need to reduce the use of fossil fuels has driven the search for more environmentally friendly methods for the acrolein synthesis and encouraged the development of new processes starting from renewable materials. In this context, one of the most well-known method is the glycerol dehydration [5–10] performed on various acidic catalysts such as tungstated titania, tungstated zirconia, supported heteropolyacids (HPA), zeolites or mixed oxides, phosphates and pyrophosphates. Indeed, crude glycerol, a three-carbon molecule, is available in the market due to its generation as a co-product in oleochemicals and biodiesel production [11] and was expected to be a rather inexpensive carbon source. Besides, the carbon footprint can be considered as much better than for the classical propylene oxidation process [6,12]. Furthermore, acrolein synthesis from glycerol could be done on site, reducing issues related to transportation or storage and minimizing the risk of accidents taking into account the toxic and flammable character of the molecule. It is well known that the two major industrial accidents linked with acrolein production, in Taft (USA) and Pierre-Bénite (France), were linked with its storage and transportation [13]. However, in spite of such interesting features, there are some drawbacks which limit the widespread adoption of this process. Firstly, volatility of glycerol prices is high. Secondly, the local glycerol availability is not sufficient to satisfy the worldwide acrolein needs even with a high glycerol dehydration yield. As glycerol production represents 10 wt % of the biodiesel production, it requires the equivalent of one million tons of biodiesel to produce 100 kt glycerol that would allow about 50 kt acrolein. If this route remains appropriate for small acrolein plants, the stable supply for larger plants needs to be guaranteed. In

* Corresponding author.
*E-mail address:* aline.auroux@ircelyon.univ-lyon1.fr (A. Auroux).

https://doi.org/10.1016/j.apcatb.2019.118421
Received 28 May 2019; Received in revised form 5 November 2019; Accepted 11 November 2019
Available online 12 November 2019
0926-3373/ 

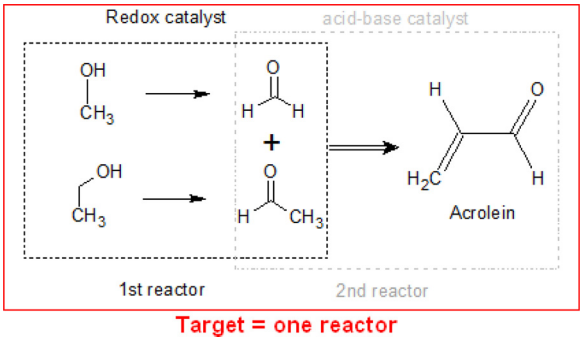


**Scheme 1.** Acrolein production by oxidative coupling of methanol and ethanol, requiring multifunctional catalysts with Redox and Acid-Base properties in a two steps process (····); in a single reactor which is the target to minimize the capital cost (−).

addition to that, despite good performances, glycerol dehydration catalysts require periodic regeneration and appropriate technologies, as glycerol dehydration leads to severe coking [14].

The oxidative coupling of alcohols has also been investigated as alternative for acrolein production using a mixture of methanol and ethanol. In this process, patented by Dubois *et al.* [15,16], the reaction can be carried out in two steps as described in Scheme 1, or preferably in a single reactor (allowing energy saving) where all the reactions are taking place at the same time. For research purposes, using two consecutive steps are more appropriate to better understand the reaction mechanism for a better optimization of the catalysts. In the first step the mixture of methanol and ethanol passes through a reactor containing an iron-molybdate catalyst (FeMoOx) in order to oxidize them to formaldehyde and acetaldehyde [17,18]. Then, for the second step, the aldehydes mixture is directly fed, without separation or addition, into another reactor containing an acid-base catalyst where cross-aldolization occurs to form acrolein [12]. It is important to note that in the oxidative coupling of alcohols process, the feedstock is at least partially bio-based. Ethanol is already produced by fermentation using agricultural resources and methanol can be produced with syngas from waste gasification [19].

Iron-molybdate catalysts are the state-of-the-art mixed oxide catalysts for methanol oxidation to formaldehyde at low alcohol partial pressure. They are also known to oxidize ethanol into acetaldehyde [20]. Dubois *et al.* [21] have patented and published that in high methanol partial pressure the same catalyst leads to the formation of dimethoxymethane (DMM, or Methylal) showing that in these conditions the catalyst should be both redox and acidic. FeMoOx has also been used [22] for selective reduction of propionaldehyde content in an acrolein stream demonstrating that it is not over oxidizing acrolein.

Various catalysts have already been investigated for the aldolization of acetaldehyde and formaldehyde in gas-phase in $O_2$ free environment: mixed oxides [1], hydrotalcites [25], zeolites [26–29], clays [24], silica [12,23,30,31] and alumina [30]. It has often been reported that the acid-base properties drive the selectivity of the reaction, but mechanism remains unclear. It is important to note that the reaction can occur both on acidic and basic sites (Scheme 2). Indeed, Azzouz and co-authors [24] have shown that basic sites enable the reaction thanks to an H-abstraction of the acetaldehyde on the α-carbon of the carbonyl sites, while an excessive quantity of acidic sites are known to influence unfavorably the selectivity to acrolein. Ai [1,32] proposed that acrolein formation is catalyzed by weak basic sites whereas strong basic sites lead to $CO_2$ and methanol production. Nonetheless Dumitriu *et al.* [25] observed that condensation occurs mainly on medium acidic strength sites.

Lilic *et al.* [12] studied the reaction in presence of oxygen. In this case, the presence of a few strong basic sites ($Q_{diff}$ > 150 kJ $mol^{-1}$) was revealed to be essential for improved acrolein production, even though an excessive amount of basic sites led to a higher production of carbon oxides. Magnesium oxide supported on silica (amphoteric catalyst) was observed to be the most active catalyst. The improved acrolein yield was explained by the additional presence of strong acidic sites. This acid-base cooperation created a positive impact on acrolein production by decreasing the unwanted production of carbon oxides. Only cross condensation of acetaldehyde and formaldehyde to acrolein was observed, while self-condensation of acetaldehyde which should lead to crotonaldehyde was not detected in the studied conditions. It was hypothesized to be due to thermodynamic considerations (equilibrium limitation), as the crotonaldehyde formation is less favoured than the acrolein formation. However, this hypothesis is not fully satisfactory. When the reverse reactions (retroaldolization) were studied by feeding acrolein or crotonaldehyde, formaldehyde nor acetaldehyde have been detected, suggesting that the equilibrium was not reached in these conditions. Therefore other factors could affect the reaction mechanism.

In another study, Lilic *et al.* [23] stated that the co-existence of strong basic and acidic sites in similar amounts (strong basic sites to strong acidic sites ratio close to 1) seems to be the best surface configuration for maximizing the acrolein production in oxidizing reaction conditions. On amphoteric catalysts, a sufficient amount of strong acidic sites enhances acrolein production and limits carbon oxide production, thus allowing the catalyst to work at higher temperatures. So it appears that the aldolization reaction is favored by cooperation between acidic and basic sites, and a balance between acidic and basic properties should be the key to the reaction [1,24–29,32,33].

The aim of this work is to correlate the acid-base properties of amphoteric mixed spinel oxide catalysts (x$Al_2O_3$-yMgO with various $Al_2O_3$/MgO ratios) to the production of acrolein through an oxidative coupling of alcohols process. The reaction has been performed in two separate fixed bed reactors in the gas phase. A redox catalyst was used for the oxidation reaction while the investigated materials here were tested as acid/base catalysts for the aldolization reaction. The acid-base and adsorptive properties of the involved catalysts were investigated by adsorption microcalorimetry using $NH_3$, $SO_2$, methanol, acetaldehyde, formaldehyde and propionaldehyde as probe molecules. Propionaldehyde is used here as the best substitute for acrolein which cannot be easily handled at the laboratory. The use of microcalorimetry technique allows the simultaneous determination of the number, strength, and strength distribution of the active sites. Other physicochemical properties were determined by using XRD, X-ray Photoelectron Spectroscopy (XPS), $^{27}$Al MAS NMR, thermal and chemical analyses, and $N_2$-adsorption at −196 °C.

## 2. Experimental

### 2.1. Catalyst characterization

Spinel catalysts (x$Al_2O_3$ yMgO) were all supplied by Baikowski. All chemicals were analytical grades purchased form Sigma-Aldrich.

XRD patterns were recorded on a Bruker D8 Advance A25 diffractometer at room temperature using $CuK_\alpha$ radiation (0.154 nm) from 4 to 80° in 0.02° steps with 0.5 s per step.

The XPS spectra were acquired by using a VG Scienta SES 200-2 spectrometer (VG Scienta, Uppsala, Sweden) equipped with a hemispherical electron analyzer and an Al anode (AlKα = 1486.6 eV) powered at 150 W, a pass energy of 100 eV, and a hybrid lens mode. The detection area analyzed was 24 $mm^2$. Charge neutralization was required for all samples. The peaks were referenced to the C−(C, H) components of the C1s band at 284.6 eV. The peak fitting to theoretical Gaussian–Lorentzian functions were performed using XPS processing software (casaXPS software 2.3.18 Ltd., Teignmouth, UK). The residual pressure in the spectrometer chamber was $10^{-9}$ mbar during data acquisition.

$^{27}$Al MAS NMR experiments were performed by accumulating 1024

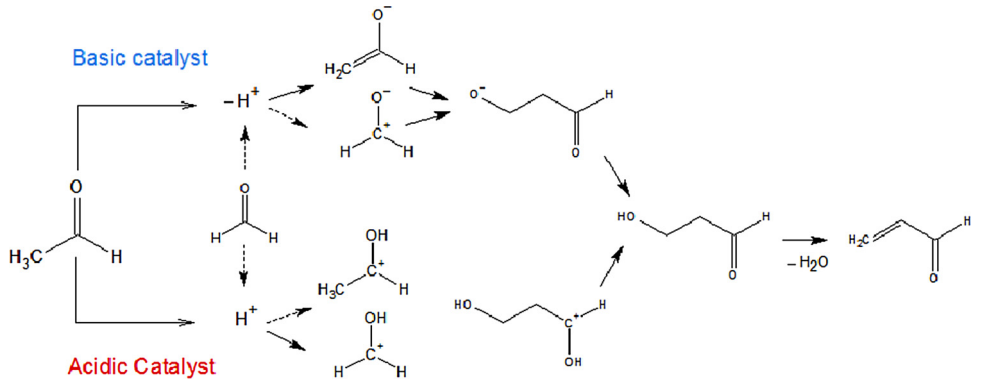


**Scheme 2.** Summary of basic and acidic reaction pathways proposed for cross-aldol condensation of formaldehyde and acetaldehyde. Adapted from [23,24].

scans with a Bruker AVANCE III 500WB spectrometer at a resonance frequency of 130.29 MHz with an excitation of π/12 pulses and a repetition time of 1 s. A commercial 4 mm double H/X/Y probe was used to perform the MAS experiments with a spinning rate of 11.5 kHz. The reference for the chemical shifts was an aqueous 1 M $Al(NO_3)_3$ solution.

Chemical analyses were performed using inductively coupled plasma optical emission spectroscopy (ICP-OES) with an ACTIVA spectrometer from Horiba JOBIN YVON. Prior to analysis, the samples were dissolved in a mixture of inorganic acids ($H_2SO_4$ + $HNO_3$) and heated to 250 − 300 °C. The amount of carbon was determined by measuring the thermal conductivity of the catalysts.

The acid/base properties of the catalysts were determined by adsorption microcalorimetry of $NH_3$ and $SO_2$. The experiments were performed at 150 °C in a Tian-Calvet heat flow calorimeter (C80 from Setaram) linked to a conventional volumetric apparatus equipped with a Barocel capacitance manometer for pressure measurements, which enables the determination of adsorbed amounts and equilibrium pressure. Each sample was pretreated in a quartz cell overnight at 400 °C under vacuum ($10^{-5}$ Pa) prior to successive introduction of small doses of probe molecule. The adsorption run was stopped at a final equilibrium pressure of 67 Pa ($V_{tot}$). After adsorption, evacuation was carried out by pumping for approximately 40 min. After outgassing, a second run of adsorption was carried out until an equilibrium pressure of 27 Pa was attained. The adsorption isotherms correlate the amount of probe molecule adsorbed with the corresponding equilibrium pressure. The first adsorption allowed us to measure the overall uptake of probe gas on catalyst. By subtracting the second isotherm from the first one, the irreversibly adsorbed amount ($V_{irrev}$) of probe gas was obtained. An estimation of the number of strong acidic and basic sites can be derived from this amount. The same experiments using $NH_3$ and $SO_2$ were also performed at 80 °C on sample $1Al_2O_3$ 1 MgO. To get additional information about Brønsted and Lewis acidity, methanol adsorption microcalorimetry experiments were performed, following the same protocol as for $NH_3$ and $SO_2$ adsorptions, at a temperature of 30 °C.

Similarly, reactants adsorption was studied at 30 °C by using formaldehyde, acetaldehyde and propionaldehyde as probe molecules. Successive adsorption of formaldehyde and acetaldehyde (reactants) has also been performed at 80 °C on sample $1Al_2O_3$ 1 MgO following the same procedure described earlier.

### 2.2. Catalytic test

Acrolein production was performed in a setup consisting of two sequential stainless-steel continuous-flow reactors (R1 and R2), the first one filled with the redox catalyst and the second one with the aldolization (acid/base) catalyst, both working close to atmospheric pressure. The two vertical reactors were heated independently by two salt baths. The reaction temperature was monitored by moving a thermocouple inserted in the catalytic bed, allowing the determination of the temperature profile and the identification of hot-spots. In the first reactor, simultaneous oxidation of ethanol and methanol (VWR Chemicals) was performed on a commercial FeMoOx catalyst (3 g) diluted with steatite (20 g) for temperature control, producing mainly acetaldehyde and formaldehyde (Reaction 1).

$CH_3CH_2OH + CH_3OH + O_2 \rightarrow CH_3CHO + HCHO + 2H_2O$ (**Reaction 1**)

The products exiting from the first reactor were directly sent into the second one, where aldol condensation of acetaldehyde and formaldehyde and then dehydration to acrolein occurred. Reaction conditions in the first reactor were optimized to obtain the highest (acetaldehyde + formaldehyde) yield and partial conversion to simulate what could happen in a single reactor. The optimal conditions, in order to limit the COx production, for the first reactor, were MeOH/EtOH/$O_2$/$N_2$ molar ratio = 4:2:8:86, $T_1$ = 266 °C, GHSV = 10,000 or 5000 $h^{-1}$. GHSV is calculated as the gas flow-rate in normal conditions divided by the estimated volume of the undiluted catalyst. In the second reactor, aldolization catalysts (20 g) were tested by varying the temperature ($T_2$) between 266 and 305 °C and the GHSV between 10,000 and 5000 $h^{-1}$ (Reaction 2). This temperature range was based on the FeMoOx catalyst operating conditions in reactor 1 keeping in mind the final aim of using only one reactor.

$CH_3CHO + HCHO \rightarrow CH_2(OH)CH_2CHO \rightarrow CH_2{=}CH\text{-}CHO + H_2O$ (**Reaction 2**)

Comparison of the catalysts was performed at conversions lower than 100%. The products exiting from the second reactor were collected in two consecutive traps (cooled to 0 °C in an ice bath). Incondensable products ($O_2$, $N_2$, CO, $CO_2$) were quantified online thanks to a micro-GC using a thermal conductivity detector (TCD) with a silica Porous Layer Open Tubular (PLOT) column to measure $CO_2$ concentration and a molecular sieves column to analyse $O_2$, $N_2$ and CO. Condensable products (acrolein, acetaldehyde, methanol, ethanol, crotonaldehyde, and others) were quantified offline by GC (ZB-WAX Plus column) equipped with a flame ionization detector. Prior to analysis, formaldehyde was derivatized in a solution of dinitrophenylhydrazine (DNPH) and then quantified offline by GC (HP-5 column) equipped with a flame ionization detector.

Conversion (C) of the reactants (methanol, ethanol, formaldehyde and acetaldehyde) and of the carbon [%], molar and carbon Yields (Y) of acrolein, acetaldehyde and formaldehyde [%], and selectivity (S) towards acrolein [%] were calculated as follows (detailed calculations are available in supplementary information):

**Conversions of reactants are calculated as above**:

$$\mathbf{C_{MeOH}\ [\%]} = (\text{mol. h}^{-1}\ \text{MeOH}_{converted}) / (\text{mol. h}^{-1}\ \text{MeOH}_{in}) \times 100\%$$

$$\mathbf{C_{EtOH}\ [\%]} = (\text{mol. h}^{-1}\ \text{EtOH}_{converted}) / (\text{mol. h}^{-1}\ \text{EtOH}_{in}) \times 100\%$$

$C_{Formaldehyde}$ [%] = (mol. $h^{-1}$ $Formaldehyde_{converted}$) / (mol. $h^{-1}$ $Formaldehdye_{in}$) x 100%

$C_{Acetaldehyde}$ [%] = (mol. $h^{-1}$ $Acetaldehyde_{converted}$) / (mol. $h^{-1}$ $Acetaldehyde_{in}$) x 100%

**Carbon conversion [%]** = ((1 x mol. $h^{-1}$ $MeOH_{converted}$) + (2 x mol. $h^{-1}$ $EtOH_{converted}$)) / (mol. $h^{-1}$ $MeOH_{in}$ + 2 $EtOH_{in}$)

**Carbon yield of acrolein is calculated as above**:

$Y_{acrolein}$ [%] = (3 mol.$h^{-1}$ $acrolein_{produced}$) / (1 mol.$h^{-1}$ $MeOH_{in}$ + 2 mol.$h^{-1}$ $EtOH_{in}$) x 100%

As the reaction conditions were chosen to obtain a MeOH/EtOH molar ratio of 2, supposing all ethanol was transformed selectively to acrolein the calculation for carbon yield of acrolein is:

$Y_{acrolein}$ [%] = (3 × 1 mol) / (2 mol MeOH + 2 × 1 mol EtOH) = ¾ = 75 %

The maximum yield of acrolein could reach 75 % at best.

For example, a 40 % yield of acrolein would represent 40/75 = 53 % of the theoretical maximum.

The selectivity is calculated as:

$S_{products}$ [%] = Y [%] / C [%]

For acrolein, this calculation can be described as:

$S_{acrolein}$ [%] = (3 x mol. $h^{-1}$ $acrolein_{produced}$) / (mol. $h^{-1}$ $MeOH_{reacted}$ + 2 x mol. $h^{-1}$ $EtOH_{reacted}$) x 100%

## 3. Results and discussion

### 3.1. Chemical and XPS analyses

Table 1 presents the studied catalysts with their specific surface areas ($S_{BET}$), sulfur contents, and the results of chemical and XPS analyses. The samples with $Al_2O_3$/MgO ratios of 3, 6 and 12) present similar specific surfaces areas (77, 74 and 77 $m^2.g^{-1}$ respectively) and higher values than sample with $Al_2O_3$/MgO ratio of 1. The sulfur contents of the samples decrease with increasing alumina content. The relatively high content of sulfur is related to the Baikowski synthesis process; however, the sulfur surface density is detectable by XPS only on sample $1Al_2O_3$ 1 MgO (1.05 At %) evidencing an enrichment of the surface in free sulfur. Similar Al/Mg ratios were determined by both chemical and XPS analyses for all catalysts except $12Al_2O_3$ 1 MgO. It is likely $12Al_2O_3$ 1 MgO powder is a more heterogeneous material when compared with the other catalysts and presents free $Al_2O_3$ as further confirmed by XRD (Fig. 1), thus arguing for a higher stoichiometry than the 1/12 ratio.

### 3.2. X-ray diffraction

Fig. 1 shows the XRD patterns of the studied samples with different Mg/Al ratios. Peaks centered at 2θ = 19, 31, 36, 45, 59 and 65° can be

**Table 1**
List of studied catalysts with surface area, sulfur content, chemical (C.A.) and XPS analyses.

| Sample | $S_{BET}$ ($m^2$ $g^{-1}$) | Sulfur (ppm) | C.A. (metal wt%) | | XPS (metal wt%) | |
|---|---|---|---|---|---|---|
| | | | Al | Mg | Al | Mg |
| $1Al_2O_3$ 1 MgO | 41 | 3275 | 36.2 | 15.3 | 37.0 | 15.4 |
| $3Al_2O_3$ 1 MgO | 77 | 2604 | 43.9 | 6.4 | 46.3 | 5.5 |
| $6Al_2O_3$ 1 MgO | 74 | 2483 | 45.6 | 3.4 | 47.1 | 3.8 |
| $12Al_2O_3$ 1 MgO | 77 | 2101 | 46.5 | 1.7 | 47.7 | 2.8 |

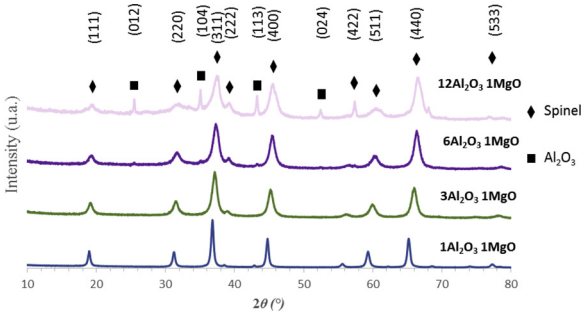


**Fig. 1.** XRD patterns of investigated spinel catalysts.

assigned to $MgAl_2O_4$ spinel. The sample with $Al_2O_3$/MgO ratio of 12 displays lower intensity and broader peaks than $1Al_2O_3$ 1 MgO, possibly indicating a weaker crystallinity and smaller size of crystallites. In this sample, spinel was not the only phase present, as peaks corresponding to α-alumina were also observed.

### 3.3. $^{27}Al$ NMR study

To confirm the identification of the catalysts, $^{27}Al$ MAS NMR spectra were recorded (Fig. 2). The spectra show two resonance lines at around 7 ppm, attributed to octahedrally coordinated $Al^{3+}$ ($Al_O$), and around 66 ppm attributed to tetrahedral $Al^{3+}$ ($Al_T$). All the other observed peaks correspond to spinning sidebands. Presence of tetrahedrally coordinated alumina could be attributed to the presence of excess alumina or an inversion of spinel phase [34].

It is apparent that $12Al_2O_3$ 1 MgO diplays a higher quantity of tetrahedrally coordinated alumina than $1Al_2O_3$ 1 MgO. Interestingly, $Al_T$ chemical shifts diminish with increasing Al/Mg ratio because of the replacement of neighborhood $Mg^{2+}$ cations by more electronegative $Al^{3+}$. All these results are in agreement with previous studies [34,35].

### 3.4. Acid-base and adsorptive properties of the catalysts

The number, strength and strength distribution of acid/base sites were determine by adsorption microcalorimetry of $NH_3$ and $SO_2$ probe molecules, respectively. It is important to note that ammonia is suitable to quantify not only Brønsted acid sites (transfer of proton from surface hydroxyls) but also Lewis sites (coordination with an electron-deficient atom such as a metal cation) [36,37]. Table 2 displays the total and irreversible (chemisorption) amounts of adsorbed ammonia and sulfur dioxide at 150 °C and 27 Pa equilibrium pressure for the studied spinels. The initial heat of adsorption and ratios of basic to acidic sites (total and chemisorption sites) are also reported. Fig. 3 displays a comparison of the strength distributions of acidic and basic sites for the investigated catalysts. Results from Fig. 3 and Table 2 confirm the amphoteric character of all samples. Heats of adsorption of $SO_2$ higher than 150 kJ.$mol^{-1}$ indicate the presence of strong basic sites probably due to

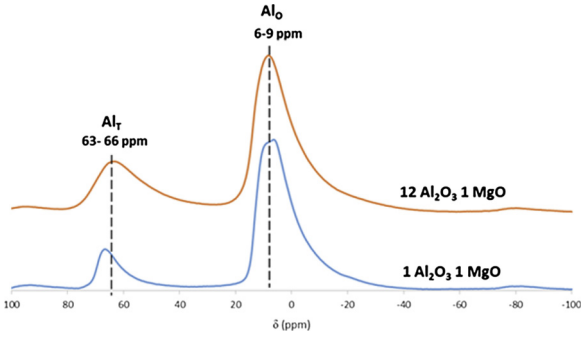


**Fig. 2.** $^{27}Al$ MAS NMR spectra of spinel catalysts.

**Table 2**
$Q_{init}$, $V_{irrev}$ and $V_{tot}$ calculated from adsorption isotherms of $SO_2$ and $NH_3$ obtained by microcalorimetry measurements at 150 °C.

| Sample | $NH_3$ | | | $SO_2$ | | | $Base_{tot}/Acid_{tot}$ [d] $V_{tot}$[b] [μmol$SO_2$. $g^{-1}$]/ $V_{tot}$ [μmol$NH_3$. $g^{-1}$] | $Base_{chem}/Acid_{chem}$ [e] $V_{irrev}$[b] [μmol$SO_2$. $g^{-1}$]/ $V_{irrev}$ [μmol$NH_3$. $g^{-1}$] |
|---|---|---|---|---|---|---|---|---|
| | $Q_{init}$[a] (kJ. $mol^{-1}$) | $V_{total}$[b] (μmol. $g^{-1}$) | $V_{irrev}$[c] (μmol. $g^{-1}$) | $Q_{init}$[a] (kJ. $mol^{-1}$) | $V_{total}$[b] (μmol. $g^{-1}$) | $V_{irrev}$[c] (μmol. $g^{-1}$) | | |
| $1Al_2O_3$ 1 MgO | 169 | 119.0 | 48,5 | 182 | 58.9 | 45.0 | 0.49 | 0.92 |
| $3Al_2O_3$ 1 MgO | 164 | 106.0 | 34.8 | 180 | 139.4 | 111.3 | 1.31 | 3.19 |
| $6Al_2O_3$ 1 MgO | 181 | 107.3 | 30.4 | 172 | 136.3 | 110.6 | 1.27 | 3.64 |
| $12Al_2O_3$ 1 MgO | 170 | 125.9 | 44.9 | 193 | 147.0 | 117.5 | 1.16 | 2.61 |

[a] Heat evolved from the first $SO_2$ or $NH_3$ dose. [b] Total amount of $SO_2$ and $NH_3$ adsorbed under an equilibrium pressure of 27 Pa. [c] Amount of chemisorbed $SO_2$ and $NH_3$ under an equilibrium pressure of 27 Pa. [d] Ratio of total basic to acidic sites. [e] Ratio of strong basic to acidic sites.

MgO which is known to be basic [36,38–42]. Between different catalysts, $12Al_2O_3$ 1 MgO presents the highest initial heat of $SO_2$ adsorption ($Q_{init}$ = 193 kJ.$mol^{-1}$) and the highest number of basic sites ($V_{tot}$ = 147 μmol.$g^{-1}$) followed by $3Al_2O_3$ 1 MgO and $6Al_2O_3$ 1 MgO (139 and 136 μmol.$g^{-1}$ respectively). $1Al_2O_3$ 1 MgO shows more than twice less basic sites (59 μmol.$g^{-1}$) when comparing with the other spinels which can be related to its low specific surface area. Regarding the strength distribution (Fig. 3), $3Al_2O_3$ 1 MgO appears to have the highest amount of strong basic sites ($Q_{diff}$ > 150 kJ.$mol^{-1}$) directly followed by $6Al_2O_3$ 1 MgO and $12Al_2O_3$ 1 MgO.

Concerning acidity, $12Al_2O_3$ 1 MgO presents the highest amount of total acidic sites (126 μmol.$g^{-1}$). Surprisingly, $1Al_2O_3$ 1 MgO spinel, presents a dominant acidic character with a total amount of $NH_3$ adsorption of 119 μmol.$g^{-1}$. It is interesting to note that $3Al_2O_3$ 1 MgO exhibits the lowest number of strong acidic sites among studied catalysts. Ratios between total amounts of basic to acidic sites, and chemisorption basic to acidic sites, have been calculated (Table 2). Although the studied magnesium aluminate spinels are amphoteric, it can be observed that, except $1Al_2O_3$ 1 MgO with a specific surface area of 41 $m^2.g^{-1}$, the catalysts display a more pronounced basic than acidic character in agreement with XPS results. Indeed, as displayed on Fig. 4, the O1s binding energy decreases with increasing number of basic sites per surface area square meters. Lower O1s binding energy is indicating electron richer element thus more basic as also reported in [43].

The adsorption microcalorimetry was further used as a powerful tool able to supply information about the strength of reactive gases-catalyst surface interactions. The direct measurement of heats of adsorption and their variation with coverage can contribute to the study of all phenomena which can be involved in one catalyzed process, e.g. activation/deactivation of the catalyst, coke production, pore blocking, sintering, etc. Therefore, to get some insight in the reaction mechanism the adsorptions of formaldehyde, acetaldehyde, propionaldehyde and methanol were performed at 30 °C for all spinel-based catalysts. Formaldehyde and acetaldehyde are the reactants in the aldolization reaction, propionaldehyde is a possible by-product in the catalytic process and methanol is one of the reactive gases used in the oxidative coupling of alcohols not completely transformed during the oxidation reaction contrary to ethanol. It is worth noticing that methanol as a H-donor can behave as a Brønsted acid and because of its pair of electrons on the oxygen it can also act as a Lewis acid.

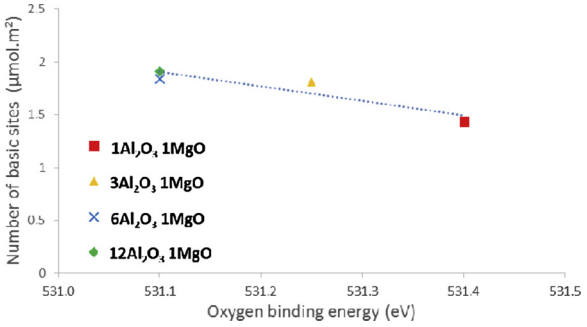


**Fig. 4.** Oxygen binding energy obtained by XPS *vs* number of total surface basic sites (expressed in μmol. $m^{-2}$).

The calorimetric results obtained at 30 °C are summarized in Tables 3 and 4 and Figs. 5, S1 - S3. Table 3 presents the initial heats of adsorption together with the total and irreversible (chemisorption) amounts of methanol adsorbed by the studied magnesium aluminate spinel catalysts at 30 °C under an equilibrium pressure of 27 Pa. All catalysts display initial heats close to 150 kJ.$mol^{-1}$ which would suggest strong associative and/or dissociative adsorption of methanol on $Al^{3+}$ and $Mg^{2+}$ sites. The differential heat profiles of methanol adsorption as a function of surface coverage are given in Fig. 5 for $1Al_2O_3$ 1 MgO and Figs. S1 - S3 for the other catalysts. The differential heats of $1Al_2O_3$ 1 MgO slightly but gradually decrease with coverage until about 100 μmol $g^{-1}$ before a steeper decrease which indicates the physisorption of undissociated methanol on weaker sites with much smaller heats of adsorption. Within a narrow domain of adsorption heats (119 – 112 kJ $mol^{-1}$) this catalyst shows an homogeneous site population of middle strength characteristic of the strong associative adsorption of methanol. These results are in agreement with those already reported in

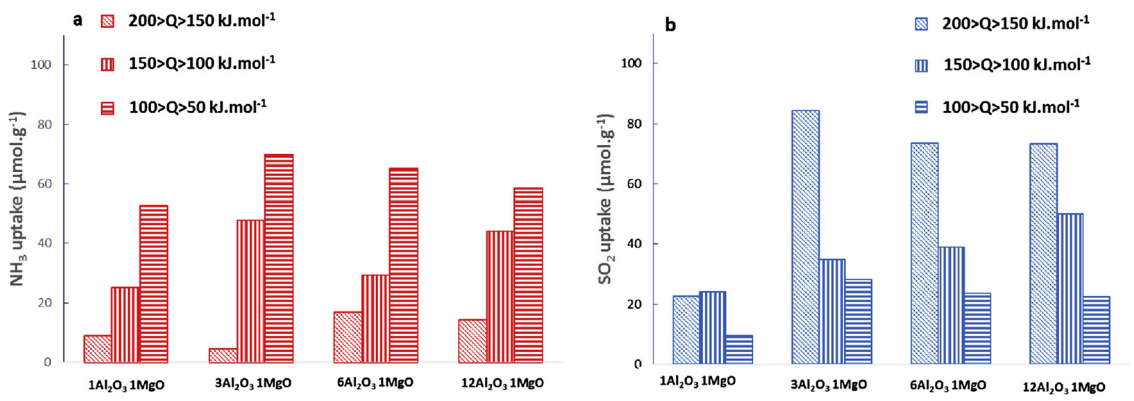


**Fig. 3.** Strength distributions of acidic (a) and basic (b) sites on fresh magnesium aluminate spinel catalysts.

**Table 3**
$Q_{init}$, $V_{irrev}$ and $V_{tot}$ calculated from adsorption isotherms of methanol obtained from microcalorimetry measurements at 30 °C.

| Sample | $Q_{init}$ [a] (kJ. mol$^{-1}$) | $V_{total}$ [b] (μmol. g$^{-1}$) | $V_{irrev}$ [c] (μmol. g$^{-1}$) |
|---|---|---|---|
| $1Al_2O_3$ 1 MgO | 144 | 218.1 | 154.7 |
| $3Al_2O_3$ 1 MgO | 150 | 442.6 | 312.0 |
| $6Al_2O_3$ 1 MgO | 149 | 431.3 | 297.3 |
| $12Al_2O_3$ 1 MgO | 140 | 462.0 | 320.7 |

[a] Heat evolved from the first methanol dose. [b] Total amount of methanol adsorbed under an equilibrium pressure of 27 Pa. [c] Amount of chemisorbed methanol under an equilibrium pressure of 27 Pa.

the literature [23,42,44,45]. Indeed, for magnesium oxide, three adsorption modes have been described based on coupled microcalorimetry - FTIR studies and DFT calculations [23,42,45–47]: i) Weak methanol adsorption, corresponding to undissociated methanol physisorbed to $Mg^{2+}$ cations and $O^{2-}$ anions, characterized by differential heats of about 60 kJ.mol$^{-1}$. ii) Strong associative adsorption of methanol presenting differential heats in the range of 95 – 125 kJ.mol$^{-1}$. iii) Finally, strong dissociative methanol adsorption characterized by differential heats between 150 and 230 kJ.mol$^{-1}$, where proton ($H^+$) and methoxy ($CH_3O$-) would be adsorbed on $O^{2-}$ and $Mg^{2+}$ on the surface.

On alumina, oxide exhibiting strong acidic Lewis type sites ($Al^{3+}$), physisorption of methanol surface has been characterized by differential heats of about 70 kJ.mol$^{-1}$, while stronger adsorption of methanol on $Al^{3+}$ cations and $O^{2-}$ anions displays differential heats in the range of 100 – 120 kJ.mol$^{-1}$. The strongest interactions correspond to chemisorption and are characterized by differential heats between 140 – 220 kJ.mol$^{-1}$ [23,44,45].

The variation of the adsorption differential heat versus coverage for magnesium aluminate spinels with ratios of alumina to magnesia of 3, 6 and 12 show similar trends, different from that observed with $1Al_2O_3$ 1 MgO (Figs. S1 – S3). The differential heats of methanol adsorption on these catalysts decrease monotonically with increasing methanol coverage without any apparent plateau characteristic for heterogeneous surfaces. Taking into account the low temperature of adsorption, this would suggest that some weaker adsorption sites were simultaneously covered together with the regular strong adsorption sites. In addition, by comparing (Table 3) the total adsorbed methanol volume ($V_{tot}$) with the irreversibly one ($V_{irr}$), it is clearly shown that most of adsorbed methanol was strongly chemisorbed (about 70 % for all catalysts). The dissociative mechanism of methanol adsorption on magnesium aluminate spinels catalysts is further supported by much larger total adsorbed and chemisorbed methanol volumes in comparison with those of $NH_3$ adsorption which titrates the surface acid sites.

The differences observed in the total and chemisorbed volumes of adsorbed methanol between $1Al_2O_3$ 1 MgO and the other samples were mostly related to differences in their surface areas although some influence of the alumina to magnesia ratio could not be completely excluded.

Fig. 5 displays differential heats of adsorption of formaldehyde, acetaldehyde, and propionaldehyde versus coverage for $1Al_2O_3$ 1 MgO, and Table 4 summarizes these data, i.e. the total and irreversible (chemisorption) amounts of aldehyde absorbed by the magnesium aluminate spinel catalysts at 30 °C under an equilibrium pressure of 27 Pa, as well as the initial heats of adsorption.

Similar shapes are observed for all adsorbates on the calorimetric curves, thus indicating that the adsorption sites are probably the same. A plateau between 120 and 140 kJ.mol$^{-1}$ is observed showing the presence of a large population of sites with high adsorption energy. It is also possible to observe that methanol, acetaldehyde and formaldehyde differential heats of adsorption are very close to each other at low coverage, while the propionaldehyde initial heat of adsorption is higher.

All the other studied catalysts display similar curves to $1Al_2O_3$ 1 MgO (Figs. S1 – S3). The initial heats of adsorption of formaldehyde are 148, 170, 164 and 168 kJ.mol$^{-1}$ for $1Al_2O_3$ 1 MgO, $3Al_2O_3$ 1 MgO, $6Al_2O_3$ 1 MgO, and $12Al_2O_3$ 1 MgO respectively (Table 4).

From Fig. 5 it can be seen that methanol is less strongly adsorbed than the aldehydes. This means that by performing the catalytic process in either a single reactor or in two consecutive reactors with only partial methanol conversion, the adsorbed alcohol on the surface of the amphoteric catalyst should be displaced by the stronger adsorption of the aldehydes.

The similar initial heats ($Q_{init}$) and chemisorbed amounts ($V_{irrev}$) for formaldehyde and acetaldehyde suggest a competitive adsorption between these two reactants. $12Al_2O_3$ 1 MgO presents the largest total adsorbed amounts of formaldehyde (634 μmol.g$^{-1}$) and acetaldehyde (571 μmol.g$^{-1}$) and also the largest amounts of strongly adsorbed aldehydes with 535 and 529 μmol.g$^{-1}$ for formaldehyde and acetaldehyde respectively. The smallest total and strongly adsorbed amounts of both aldehydes are displayed by $1Al_2O_3$ 1 MgO, probably due to its lower specific surface area as compared to the other catalysts.

The total adsorbed amount of formaldehyde is higher than those of acetaldehyde and propionaldehyde. However, the chemisorbed amount ($V_{irr}$) of formaldehyde is quite close to the chemisorbed amount of acetaldehyde. Physisorption is usually ascribed to heats of adsorption lower than 80 kJ.mol$^{-1}$. However, the presence of dimers of formaldehyde formed during physical adsorption on the solid by hydrogen bonds could explain this higher total adsorption volume at 30 °C. It also appears that the adsorption heat of propionaldehyde is always higher than that of acetaldehyde. However, the adsorbed amounts are nearly the same. The higher heats of adsorption can be explained by the difference in proton affinity, which is higher for propionaldehyde (786 kJ.mol$^{-1}$) than acetaldehyde (768.5 kJ.mol$^{-1}$): the higher the proton affinity, the higher the energy of adsorption onto the solid. Considering the proton affinity of acrolein (797 kJ.mol$^{-1}$) and crotonaldehyde (830 kJ.mol$^{-1}$), it can be deduced that their adsorption heats should be close, and higher than those of propionaldehyde. Lower adsorbed amount of propionaldehyde could be explained by some steric hinderance.

**Table 4**
Qinit, Virrev and Vtot calculated from adsorption isotherms of formaldehyde, acetaldehyde and propionaldehyde obtained from microcalorimetry measurements at 30 °C.

| Sample | Formaldehyde | | | Acetaldehyde | | | Propionaldehyde | | |
|---|---|---|---|---|---|---|---|---|---|
| | $Q_{init}$ [a] (kJ. mol$^{-1}$) | $V_{total}$ [b] (μmol. g$^{-1}$) | $V_{irrev}$ [c] (μmol. g$^{-1}$) | $Q_{init}$ [a] (kJ. mol$^{-1}$) | $V_{total}$ [b] (μmol. g$^{-1}$) | $V_{irrev}$ [c] (μmol. g$^{-1}$) | $Q_{init}$ [a] (kJ. mol$^{-1}$) | $V_{total}$ [b] (μmol. g$^{-1}$) | $V_{irrev}$ [c] (μmol. g$^{-1}$) |
| $1Al_2O_3$ 1 MgO | 148 | 291.9 | 232.4 | 151 | 257.6 | 233.0 | 184 | 274.3 | 237.6 |
| $3Al_2O_3$ 1 MgO | 170 | 598.8 | 517.4 | 156 | 554.4 | 513.4 | 173 | 564.2 | 489.7 |
| $6Al_2O_3$ 1 MgO | 164 | 566.1 | 475.5 | 154 | 537.3 | 504.5 | 168 | 518.3 | 444.5 |
| $12Al_2O_3$ 1 MgO | 168 | 633.7 | 534.8 | 172 | 571.4 | 529.0 | 182 | 563.8 | 485.3 |

[a] Heat evolved from the first formaldehyde or Acetaldehyde dose. [b] Total amount of formaldehyde and acetaldehyde adsorbed under an equilibrium pressure of 27 Pa. [c] Amount of chemisorbed formaldehyde and acetaldehyde under an equilibrium pressure of 27 Pa.

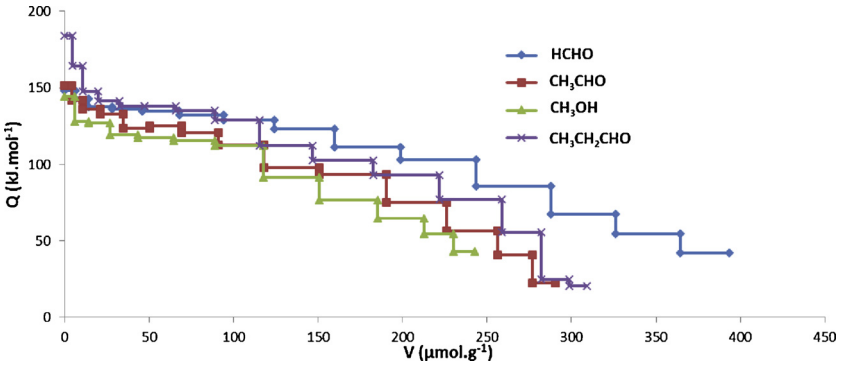


**Fig. 5.** Differential heats of adsorption of formaldehyde (blue) acetaldehyde (red), propionaldehyde (purple) and methanol (green) versus coverage for $1Al_2O_3$ 1 MgO at 30 °C. (For interpretation of the references to colour in this figure legend, the reader is referred to the web version of this article).

It is worth noticing that at room temperature, an average heat of adsorption is measured since the probe bound to both weak and strong sites simultaneously. At higher temperatures (80 − 150 °C), the probe is more selective and primarily doses the strongest sites. In order to better discriminate sites and understand the formaldehyde adsorption results, the adsorption microcalorimetry experiments of formaldehyde, acetaldehyde, ammonia and $SO_2$ have also been carried out at 80 °C on $1Al_2O_3$ 1 MgO sample.

Fig. 6 displays the adsorption isotherms (a) and differential heats (b) obtained at 80 °C. It can be seen that the adsorbed volumes of acetaldehyde and formaldehyde are now equivalent, suggesting the absence at this temperature of the formaldehyde dimers seen during adsorption of formaldehyde at 30 °C. From these isotherms, it is also apparent that the adsorbed volumes of aldehydes correspond to the sum of the adsorbed volumes of ammonia and $SO_2$, providing evidence that aldehydes do adsorb on both acidic and basic sites. Interestingly, it can be observed that formaldehyde and acetaldehyde adsorptions are more energetic than adsorption of $SO_2$. However, in reaction conditions, a small inhibition effect of $SO_2$ on the acrolein production was reported [12], probably due to the formation of sulfite and sulfates chemisorbed species in presence of water poisoning the surface.

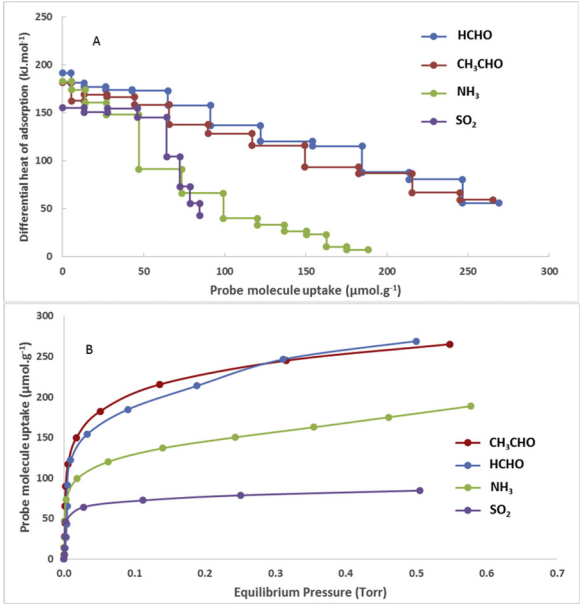


**Fig. 6.** Differential heats (A) and isotherms (B) of adsorption of acetaldehyde (red), formaldehyde (blue), ammonia (green) and $SO_2$ (purple) at 80 °C for $1Al_2O_3$ 1 MgO sample. (For interpretation of the references to colour in this figure legend, the reader is referred to the web version of this article).

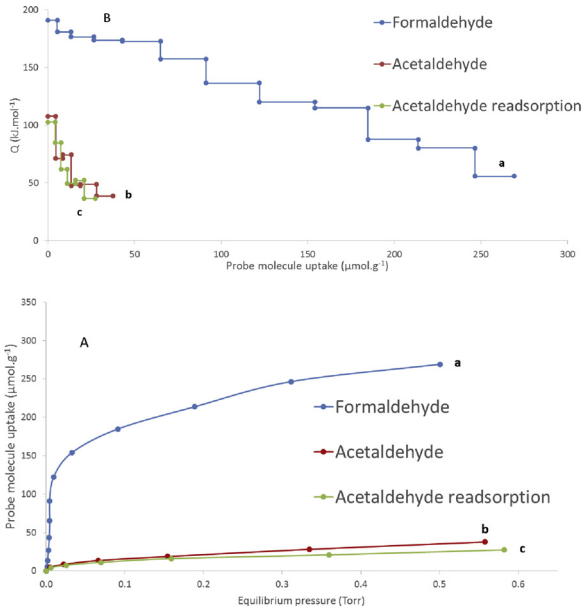


**Fig. 7.** Isotherms (A) and differential heats (B) of adsorption (a) of formaldehyde followed by adsorption (b) and readsorption (c) of acetaldehyde at 80 °C on $1Al_2O_3$ 1 MgO catalyst.

### 3.5. Consecutive adsorptions of acetaldehyde and formaldehyde

In order to study the competitive adsorption of acetaldehyde and formaldehyde, formaldehyde was first adsorbed on $1Al_2O_3$ 1 MgO sample at 80 °C (curve *a* in Fig. 7). Then, after evacuation of the physisorbed amount, adsorption of acetaldehyde was then performed (curve *b*) at the same temperature followed by desorption and readsorption of acetaldehyde (curve *c*). The opposite experiment, adsorption of acetaldehyde (curve *a* in Fig. 8) followed by adsorption (*b*) and readsorption (*c*) of formaldehyde, was also performed. Both isotherms and differential heats of adsorption are given in Figs. 7 and 8.

Adsorption and readsorption of acetaldehyde after formaldehyde adsorption evidenced that there was no chemisorption of acetaldehyde possible after saturation of strong sites by formaldehyde (curves b and c superimposed in Fig. 7). In Fig. 7, it is questionable to consider if an exchange between the adsorbed vapor (formaldehyde) and the new dose (acetaldehyde) can occur. In such a case, there would be no variation of pressure recorded during the process and a desorption peak (endothermic) would occur before the adsorption of the second probe. This phenomenon was not observed and both curves remain in the physisorption domain. On the contrary, it can be seen that after saturation by the acetaldehyde, formaldehyde can still be adsorbed and adsorption is not completely reversible (curves b and c separated in

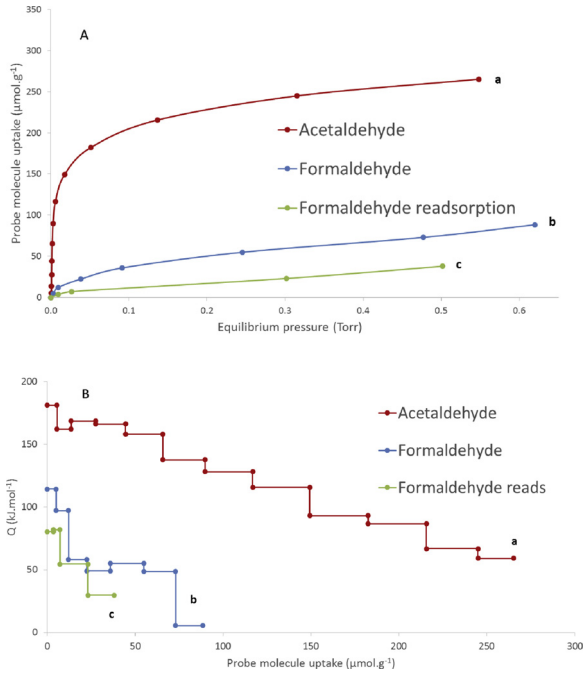


**Fig. 8.** Isotherms (A) and differential heats (B) of adsorption (a) of acetaldehyde followed by adsorption (b) and readsorption (c) of formaldehyde at 80 °C on $1Al_2O_3$ 1 MgO catalyst.

Fig. 8). This could be explained by a displacement of acetaldehyde by formaldehyde. Indeed, the initial heat of adsorption of formaldehyde (191 kJ.mol$^{-1}$) is higher than that of acetaldehyde (181 kJ.mol$^{-1}$) (Fig. 6), and the differential heats of adsorption *vs* coverage are always higher for formaldehyde. Thus acetaldehyde may be displaced by formaldehyde over a fraction of the sites (about 30 µmol.g$^{-1}$). These findings suggest that the catalysts have a stronger affinity for formaldehyde than for acetaldehyde and might result in the absence of crotonaldehyde during catalytic tests (*vide infra*).

In Fig. 8, it can be observed that the amount corresponding to the adsorbed formaldehyde (after acetaldehyde adsorption) is about the same as the number of basic sites titrated by $SO_2$ (Fig. 6). The surface is saturated either with formaldehyde (Fig. 7) or acetaldehyde (Fig. 8) with about the same amount, 270 µmol.g$^{-1}$. This suggests that acetaldehyde adsorbs like formaldehyde from the aldehyde group only, dissociatively or not. So there would remain no room left for further adsorption; however when formaldehyde is added after acetaldehyde, a noticeable amount can be adsorbed. This suggests that formaldehyde is activated when approaching the acetaldehyde layer and reacts with it forming an adsorbed hydroxypropanaldehyde molecule that would desorb later as acrolein. As the amount of formaldehyde seems to correspond to the number of titrated basic sites, does it correspond to a base catalyzed aldol reaction? (Scheme 2)

### 3.6. Catalytic tests

Acrolein can already be synthesized over iron molybdate catalysts (FeMoOx) [17]. However, the addition of an aldolization catalyst seems necessary in order to provide basic sites and improve acrolein production by cross-aldolization of formaldehyde and acetaldehyde. Magnesium aluminate spinels have been investigated as catalysts for the production of acrolein starting from a mixture of methanol (MeOH) and ethanol (EtOH) in oxidizing conditions, with the oxidation of methanol and ethanol being carried out in a first reactor under conditions already optimized to achieve the best parameters for a higher acrolein yield [12].

The molar ratio of MeOH/EtOH/$O_2$/$N_2$ was fixed at 4/2/8/86, with GHSV of 5000 h$^{-1}$ or 10,000 h$^{-1}$ and a temperature of 266 °C, for the oxidation of a mixture of methanol and ethanol in reactor 1 over FeMoOx catalyst. Under these conditions, the mixture of alcohols is not completely converted in reactor 1. For 10,000 h$^{-1}$, methanol conversion is maintained at 53 % and ethanol conversion at 76 %. Acrolein was produced with a yield of 8 % and the formaldehyde and acetaldehyde yields were 14 and 23 % respectively. The results are displayed in Fig. 9. For 5000 h$^{-1}$, the conversion of methanol is maintained at 69 % while ethanol conversion is at 90 %. Acrolein yield was 13 % (with a selectivity of 15 %) and formaldehyde and acetaldehyde were produced with 21 and 13 % yields respectively. Total carbon oxide production was 4.5 % and 5.5 % for GHSV of 5000 and 10,000 h$^{-1}$ respectively.

After reactor 1, the gas mixture was directly sent into a second reactor to undergo aldolization followed by dehydration to produce acrolein. Tests have been done at 266 °C and 285 °C with two different GHSV (5000 and 10,000 h$^{-1}$ respectively). It was found that acrolein production was enhanced by increasing the temperature. However this enhancement was accompanied by a higher production of carbon oxides. A possible model of decarboxylation reaction can be summarized as:

$$B^+ HO^- + R\text{-}CH_2\text{-}CHO \rightarrow RCH_2COO^- B^+ + 2\ H_{surface}$$

$$H_{surface} + \tfrac{1}{2}\ O_2 \rightarrow H_2O \quad \textbf{(Reaction 3)}$$

$$RCH_2COO^- B^+ + O_2 \rightarrow CO_2 + RCHO + B^+ HO^-$$

So in case of excess base, an oxidation reaction could take place, without necessarily gaseous $H_2$ production as all the reaction could take place on adsorbed phase.

Figs. 10 and S5 to S7 present the detailed results of tests performed

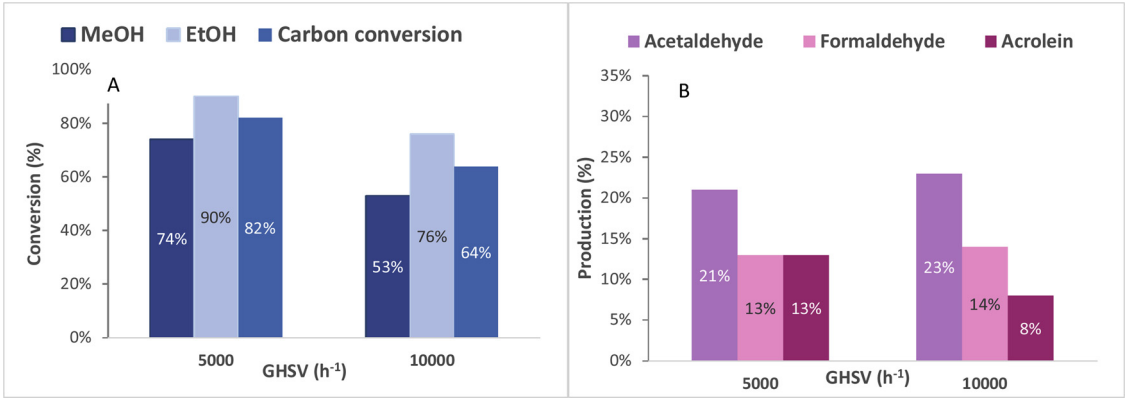


**Fig. 9.** Conversion of methanol and ethanol and carbon conversion (including methanol + ethanol) (A) and production of acetaldehyde, formaldehyde and acrolein (B) at the output of R1 (detailed calculations are available in supplementary information).

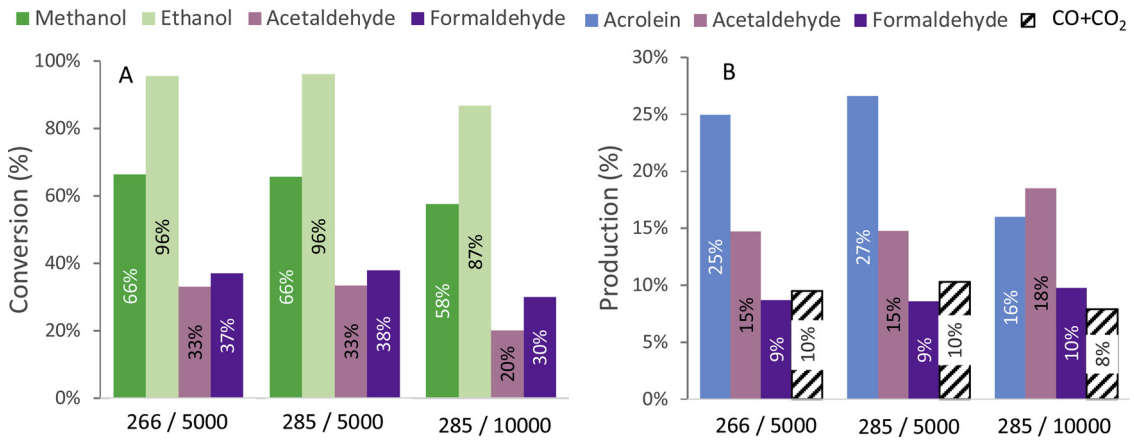


**Fig. 10.** Conversion of methanol, ethanol acetaldehyde and formaldehyde (A) and production of acrolein, acetaldehyde and CO + $CO_2$ (B) at the outlet of R2 for 1 $Al_2O_3$ 1 MgO. The x-axis show the experimental conditions used: temperature (°C)/GHSV($h^{-1}$). Formaldehyde conversion calculation integrates also the formaldehyde polymerization.

under oxidizing conditions over the four spinel catalysts at 266 and 285 °C with a GHSV of 5000 and 10,000 $h^{-1}$. The most important obtained products are acrolein, acetaldehyde, formaldehyde and carbon oxides. Traces of crotonaldehyde, propionaldehyde, acetic acid and others were also detected by gas chromatography. Production of paraformaldehyde (white powder) and of acrolein polymer was also observed, which explains the carbon balance between 80 and 90 mol % and the differences in results of formaldehyde production and conversion. Based on the co-adsorption calorimetric results, the absence of quantifiable crotonaldehyde in the products was expected and can be explained by the saturation of the catalyst surface with formaldehyde while the adsorption sites for acetaldehyde are isolated. Then when an acetaldehyde molecule adsorbs, it is surrounded by adsorbed formaldehyde, and it can only lead to acrolein and not to crotonaldehyde.

Among the studied catalysts, 1$Al_2O_3$ 1 MgO spinel obtained the best acrolein production, with 27 % yield (or 27/75 = 36 % of the theoretical maximum) with 33 % selectivity and 10 % of CO + $CO_2$ at 285 °C with a GHSV of 5000 $h^{-1}$ (Fig. 10). The second best catalyst was 12$Al_2O_3$ 1 MgO with 24 % acrolein yield with 29 % selectivity and 10 % of $CO_x$ (Fig. S5). 3$Al_2O_3$ 1 MgO also gave rise to a 24 % acrolein yield, but with a higher production of carbon oxides, 15 % (Fig. S6). 6$Al_2O_3$ 1 MgO displayed the lowest acrolein yield with 23 %, and 13 % carbon oxides production (Fig. S7). All these results were obtained at 285 °C with a GHSV of 5000 $h^{-1}$, and Fig. S8 summarizes the best results obtained at these conditions for each studied spinel catalyst. In these experiments, the acrolein yield is limited by the choice made to operate at low conversion in order to understand the reaction mechanisms that take place, especially if all the reactions would be carried out in a single reactor.

### 3.7. Characterization of the used catalysts and discussion

Physicochemical characterizations were performed on the used catalysts after catalytic testing. The specific surface areas and XRD results did not change. The color of the used catalyst after 5 h was brown, whereas fresh catalyst was white. Chemical analysis allowed us to see the presence of 1.1, 2.1, 2.0, 2.3 wt% carbon on samples 1$Al_2O_3$ 1 MgO, 3$Al_2O_3$ 1 MgO, 6$Al_2O_3$ 1 MgO, 12$Al_2O_3$ 1 MgO respectively after 5 h of reaction. After 24 h of reaction, sample 12$Al_2O_3$ 1 MgO displayed 3 wt% of carbon. In addition, $NH_3$ and $SO_2$ adsorption microcalorimetry experiments were performed on used catalysts.

Fig. 11 represents the differential heats of adsorption of ammonia (right) and $SO_2$ (left) for fresh 12$Al_2O_3$ 1 MgO (blue) and used 12$Al_2O_3$ 1 MgO after 5 h (green) and 24 h working (red). It can be seen that the number and strength of acidic sites on the used catalysts were much lower than on the fresh spinel. The acidity decreased sharply after 5 h use, but subsequently remained stable until 24 h use. The used catalysts still contained weak acidic sites (Qdiff < 80 kJ.$mol^{-1}$) in important amounts. Concerning the basicity, the decrease in number and strength of sites is even more marked than for acidity. The used magnesium aluminate spinel 12$Al_2O_3$ 1 MgO showed almost no basic sites. Contrary to acidity, the decrease of basicity continues even after 5 h, and the residual basicity after 24 h working is very weak. Basic sites are consumed during the reaction, but are needed, while acid sites are unaffected after 5 h reaction. Nonetheless, yields of acrolein at 3, 5 and 24 h are equal to 24, 23 and 23 % respectively with a decreasing acetaldehyde conversion (38, 36 and 28 %). This suggests that coke deposition seems to preferentially poison the basic sites, while acrolein production is able to continue thanks to the presence of acidic sites, confirming previous studies [12].

Thus, considering results of aldehydes consecutive adsorptions and the poisoning versus time study, both kinds of sites are necessary for an optimal reaction. A small number of basic sites appears necessary to initiate the reaction, despite their tendency to a COx overyield as shown in reaction 3. All the studied catalysts display very strong basic sites ($Q_{diff}$ > 150 kJ.$mol^{-1}$). The spinels with alumina to magnesia ratios of 3, 6 and 12 contain similar amounts of strong basic sites (Table 2), and presented similar acrolein yields. Nonetheless it can be seen on Fig. 3 that 3$Al_2O_3$ 1 MgO, which shows the highest carbon oxide production, does not exhibit very strong acidic sites ($Q_{diff}$ > 150 kJ.$mol^{-1}$), especially compared to 12$Al_2O_3$ 1 MgO. It can be deduced that the presence of strong acidic sites could have a positive influence by limiting the production of carbon oxides.

To summarize these remarks about acid-base properties, Fig. 12 displays the acrolein yield and carbon oxide production versus the ratio of strong basic to strong acidic sites for the fresh and used studied spinel catalysts. There is a drastic decreasing in the ratio of basic to acidic sites after 5 h reaction (used catalysts) compared to the fresh catalysts as already observed in Fig. 11. It is apparent that an increase in basicity/acidity results in a decrease in acrolein production and an increase in the carbon oxide yield. The best results were obtained with 1$Al_2O_3$ 1 MgO which is also the only predominantly acidic catalyst. 12$Al_2O_3$ 1 MgO and 3$Al_2O_3$ 1 MgO show similar acrolein yields, however, their acid-base profiles are different as they both present strong basic sites ($Q_{diff}$ > 150 kJ.$mol^{-1}$) but the 3$Al_2O_3$ 1 MgO catalyst does not have as much strong acidic sites and so presents a more basic profile than 12$Al_2O_3$ 1 MgO. This more basic character is probably the reason for the higher carbon oxides production. As in the case of the fresh catalysts, it can be observed again for the used catalysts that an increase of basicity seems to decrease the acrolein production. These results, in accordance with previous studies done over silica supported catalysts [12], underline the important role of acid-base properties in acrolein

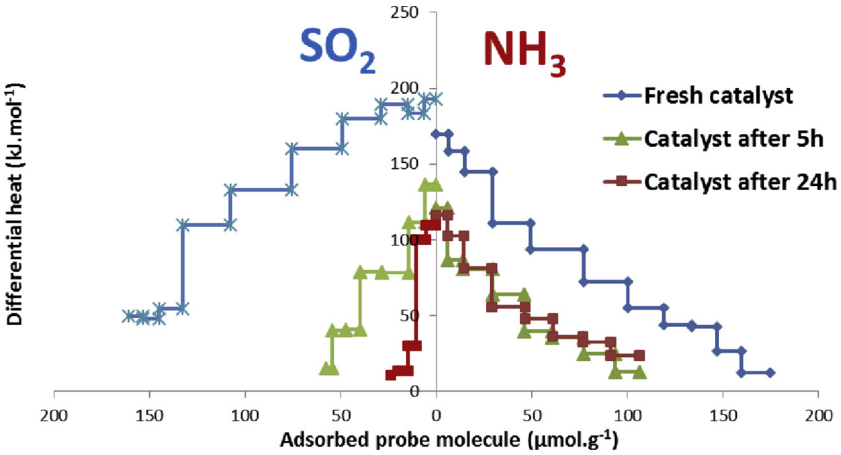


**Fig. 11.** Differential heats of adsorption of ammonia (right) and $SO_2$ (left) for fresh $12Al_2O_3$ 1 MgO (blue) and used $12Al_2O_3$ 1 MgO after 5 h (green) and 24 h (red) at 150 °C. (For interpretation of the references to colour in this figure legend, the reader is referred to the web version of this article).

production and the necessary cooperation between acidic and basic sites during the reaction.

## 4. Conclusion

The physico-chemical properties of magnesium aluminate spinel catalysts were determined by $N_2$ sorption, chemical analysis, XRD, XPS, $^{27}Al$ MAS NMR and adsorption microcalorimetry of various probe molecules ($NH_3$, $SO_2$, methanol, formaldehyde, acetaldehyde and propionaldehyde). All these properties were linked to catalytic activities for acrolein production under oxidizing conditions. The acrolein yield and carbon oxide production were correlated with the balance between acidic and basic sites of the aldolization catalysts. Enhancing acidity leads to a decrease in over-oxidation, whereas an excessive basicity decreases the acrolein production. Magnesium aluminate spinel $1Al_2O_3$ 1 MgO showed the best catalytic performance of the studied catalysts. Microcalorimetry experiments on used catalysts evidenced the beneficial participation of acidic sites in the reaction. The cooperation between acidic and basic sites seems to be one of the keys to increase acrolein production. The major products of synthesis were acrolein, acetaldehyde, formaldehyde, methanol and ethanol. Crotonaldehyde, a product of acetaldehyde self-aldolization, was detected only as traces during catalytic tests. Adsorption microcalorimetry of acetaldehyde and formaldehyde probes evidenced a better affinity of the catalysts for formaldehyde than acetaldehyde. This might explain the practically absence of crotonaldehyde as acetaldehyde would be isolated on the surface. However, even if these catalysts offer an interesting way to synthetize acrolein, the yields are still low. However, our results led to a better comprehension of the acid-base properties and reactants affinity of amphoteric catalytic materials and will help to improve the selectivity to acrolein by tuning the surface acid-base properties.

## Declaration of Competing Interest

The authors declare that they have no known competing financial interests or personal relationships that could have appeared to influence the work reported in this paper.

## Acknowledgments

The authors acknowledge the scientific services of IRCELYON. Drs. Philippe Auroy and Lionel Bonneau from Baikowski are also acknowledged for spinel catalysts supply and discussion. Dr. Simona Bennici and Mrs. Samar Hajjar (IS2M Mulhouse) are gratefully acknowledged for their contribution to the XPS analyses

## Appendix A. Supplementary data

Supplementary material related to this article can be found, in the online version, at doi:https://doi.org/10.1016/j.apcatb.2019.118421.

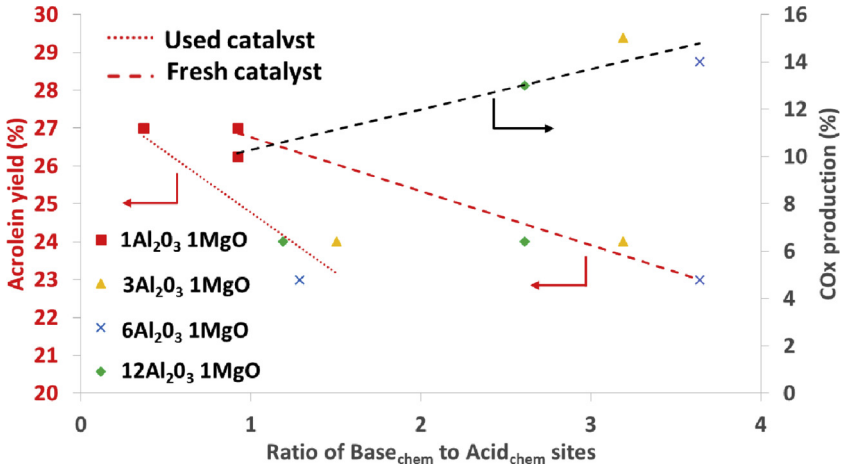


**Fig. 12.** Acrolein yield (for fresh and used catalyst) and carbon oxides production (for fresh catalyst) versus ratio of strong basic to strong acidic sites for the studied spinel catalysts.

## References


[1] M. Ai, Formation of acrylaldehyde by vapor-phase aldol condensation 1. Basic oxide catalysts, Bull. Chem. Soc. Jpn. 64 (1991) 1341–1345, https://doi.org/10.1246/bcsj.64.1342.

[2] L. Liu, X.P. Ye, J.J. Bozell, A comparative review of petroleum-based and bio-based acrolein production, ChemSusChem 5 (2012) 1162–1180, https://doi.org/10.1002/cssc.201100447.

[3] R.K. Grasselli, F. Trifirò, Acrolein and acrylic acid from biomass, Rend. Lincei 28 (2017) 59–67, https://doi.org/10.1007/s12210-017-0610-6.

[4] D. Arntz, A. Fischer, M. Höpp, S. Jacobi, J. Sauer, T. Ohara, T. Sato, N. Shimizu, H. Schwind, Acrolein and methacrolein, in: Wiley-VCH Verlag GmbH & Co. KGaA (Ed.), Ullmanns Encycl. Ind. Chem. Wiley-VCH Verlag GmbH & Co. KGaA, Weinheim, Germany, 2007, , https://doi.org/10.1002/14356007.a01_149.pub2.

[5] D. Cespi, F. Passarini, G. Mastragostino, I. Vassura, S. Larocca, A. Iaconi, A. Chieregato, J.-L. Dubois, F. Cavani, Glycerol as feedstock in the synthesis of chemicals: a life cycle analysis for acrolein production, Green Chem. 17 (2015) 343–355, https://doi.org/10.1039/C4GC01497A.

[6] M. Dalil, D. Carnevali, M. Edake, A. Auroux, J.-L. Dubois, G.S. Patience, Gas phase dehydration of glycerol to acrolein: coke on WO3/TiO2 reduces by-products, J. Mol. Catal. Chem. 421 (2016) 146–155, https://doi.org/10.1016/j.molcata.2016.05.022.

[7] A. Neher, T. Haas, D. Arntz, H. Klenk, W. Girke, US19955387720A, 1995.

[8] J.L. Dubois, C. Duquenne, W. Holderlich, US7396962B1, 2006.

[9] Q. Xie, S. Li, R. Gong, G. Zheng, Y. Wang, P. Xu, Y. Duan, S. Yu, M. Lu, W. Ji, Y. Nie, J. Ji, Microwave-assisted catalytic dehydration of glycerol for sustainable production of acrolein over a microwave absorbing catalyst, Appl. Catal. B Environ. 243 (2019) 455–462, https://doi.org/10.1016/j.apcatb.2018.10.058.

[10] F. Cavani, S. Guidetti, L. Marinelli, M. Piccinini, E. Ghedini, M. Signoretto, The control of selectivity in gas-phase glycerol dehydration to acrolein catalysed by sulfated zirconia, Appl. Catal. B Environ. 100 (2010) 197–204, https://doi.org/10.1016/j.apcatb.2010.07.031.

[11] B. Katryniok, S. Paul, V. Bellière-Baca, P. Rey, F. Dumeignil, Glycerol dehydration to acrolein in the context of new uses of glycerol, Green Chem. 12 (2010) 2079, https://doi.org/10.1039/c0gc00307g.

[12] A. Lilić, S. Bennici, J.-F. Devaux, J.-L. Dubois, A. Auroux, Influence of catalyst Acid/Base properties in acrolein production by oxidative coupling of ethanol and methanol, ChemSusChem 10 (2017) 1916–1930, https://doi.org/10.1002/cssc.201700230.

[13] ARIA (Analysis, Research and Information on Accidents) database https://www.aria.developpement-durable.gouv.fr/?s=acroléine, (Accessed March, 15th 2019).

[14] D. Sun, Y. Yamada, S. Sato, W. Ueda, Glycerol as a potential renewable raw material for acrylic acid production, Green Chem. 19 (2017) 3186–3213, https://doi.org/10.1039/C7GC00358G.

[15] J.L. Dubois, M. Capron, F. Dumeignil, US9365478B2, 2016.

[16] J.L. Dubois, US9714205B2, 2017.

[17] A. Borowiec, J.F. Devaux, J.L. Dubois, L. Jouenne, M. Bigan, P. Simon, M. Trentesaux, J. Faye, M. Capron, F. Dumeignil, An acrolein production route from ethanol and methanol mixtures over FeMo-based catalysts, Green Chem. 19 (2017) 2666–2674, https://doi.org/10.1039/C7GC00341B.

[18] A. Borowiec, A. Lilić, J.-C. Morin, J.-F. Devaux, J.-L. Dubois, S. Bennici, A. Auroux, M. Capron, F. Dumeignil, Acrolein production from methanol and ethanol mixtures over La- and Ce-doped FeMo catalysts, Appl. Catal. B Environ. 237 (2018) 149–157, https://doi.org/10.1016/j.apcatb.2018.05.076.

[19] N.S. Shamsul, S.K. Kamarudin, N.A. Rahman, N.T. Kofli, An overview on the production of bio-methanol as potential renewable energy, Renew. Sustain. Energy Rev. 33 (2014) 578–588, https://doi.org/10.1016/j.rser.2014.02.024.

[20] P.G. Pries De Oliveira, J.G. Eon, C. Moraes, L. Gorenstin Appel, Catalisadores promissores para a oxidação seletiva do etanol, Inf. Int. 17 (1985) 25–30.

[21] J.L. Dubois, US9145349B2, 2013.

[22] J.F. Devaux, J.L. Dubois, Process for manufacturing acrolein/acrylic acid, US9296676B2, 2012.

[23] A. Lilić, T. Wei, S. Bennici, J.-F. Devaux, J.-L. Dubois, A. Auroux, A comparative study of basic, amphoteric, and acidic catalysts in the oxidative coupling of methanol and ethanol for acrolein production, ChemSusChem 10 (2017) 3459–3472, https://doi.org/10.1002/cssc.201701040.

[24] A. Azzouz, D. Messad, D. Nistor, C. Catrinescu, A. Zvolinschi, S. Asaftei, Vapor phase aldol condensation over fully ion-exchanged montmorillonite-rich catalysts, Appl. Catal. Gen. 241 (2003) 1–13, https://doi.org/10.1016/S0926-860X(02)00524-0.

[25] E. Dumitriu, V. Hulea, C. Chelaru, C. Catrinescu, D. Tichit, R. Durand, Influence of the acid–base properties of solid catalysts derived from hydrotalcite-like compounds on the condensation of formaldehyde and acetaldehyde, Appl. Catal. Gen. 178 (1999) 145–157, https://doi.org/10.1016/S0926-860X(98)00282-8.

[26] C. Cobzaru, S. Oprea, E. Dumitriu, V. Hulea, Gas phase aldol condensation of lower aldehydes over clinoptilolite rich natural zeolites, Appl. Catal. Gen. 351 (2008) 253–258, https://doi.org/10.1016/j.apcata.2008.09.024.

[27] E. Dumitriu, V. Hulea, I. Fechete, A. Auroux, J.-F. Lacaze, C. Guimon, The aldol condensation of lower aldehydes over MFI zeolites with different acidic properties, Microporous Mesoporous Mater. 43 (2001) 341–359, https://doi.org/10.1016/S1387-1811(01)00265-7.

[28] E. Dumitriu, V. Hulea, N. Bilba, G. Carja, A. Azzouz, Synthesis of acrolein by vapor phase condensation of formaldehyde and acetaldehyde over oxides loaded zeolites, J. Mol. Catal. 79 (1993) 175–185, https://doi.org/10.1016/0304-5102(93)85100-8.

[29] A. Ungureanu, S. Royer, T.V. Hoang, D. Trong On, E. Dumitriu, S. Kaliaguine, Aldol condensation of aldehydes over semicrystalline zeolitic-mesoporous UL-ZSM-5, Microporous Mesoporous Mater. 84 (2005) 283–296, https://doi.org/10.1016/j.micromeso.2005.05.038.

[30] W.J. Palion, S. Malinowski, Gas phase reactions of acetaldehyde and formaldehyde in the presence of mixed solid catlysts containing silica and alumina, React. Kinet. Catal. Lett. 1 (1974) 461–465, https://doi.org/10.1007/BF02074480.

[31] S. Malinowski, S. Basinski, Kinetics of aldolic reactions in the gaseous phase on solid catalysts of basic character, J. Catal. 2 (1963) 203–207, https://doi.org/10.1016/0021-9517(63)90044-7.

[32] M. Ai, Formation of acryladehyde by vapor-phase aldol condensation II. Phosphate catalysts, Bull. Chem. Soc. Jpn. 64 (1991) 1346–1350, https://doi.org/10.1246/bcsj.64.1346.

[33] E. Dumitriu, N. Bilba, M. Lupascu, A. Azzouz, V. Hulea, G. Cirje, D. Nibou, Vapor-phase condensation of formaldehyde and acetaldehyde into acrolein over zeolites, J. Catal. 147 (1994) 133–139, https://doi.org/10.1006/jcat.1994.1123.

[34] Roberta L. Millard, Ronald C. Peterson, Brian K. Hunter, Temperature dependence of cation disorder in $MgAl_2O_4$ spinel using $^{27}Al$ and $^{17}O$ magic-angle spinning NMR, Am. Mineral. 77 (1992) 44–52.

[35] V. Diez, Effect of the chemical composition on the catalytic performance of MgyAlOx catalysts for alcohol elimination reactions, J. Catal. 215 (2003) 220–233, https://doi.org/10.1016/S0021-9517(03)00010-1.

[36] A. Auroux, A. Gervasini, Microcalorimetric study of the acidity and basicity of metal oxide surfaces, J. Phys. Chem. 94 (1990) 6371–6379, https://doi.org/10.1021/j100379a041.

[37] A. Auroux, A. Gervasini, C. Guimon, Acidic character of metal-loaded amorphous and crystalline silica – Aluminas determined by XPS and adsorption calorimetry, J. Phys. Chem. B 103 (1999) 7195–7205, https://doi.org/10.1021/jp990243h.

[38] A. Gervasini, G. Bellussi, J. Fenyvesi, A. Auroux, Microcalorimetric and catalytic studies of the acidic character of modified metal oxide surfaces. 1. Doping ions on alumina, magnesia, and silica, J. Phys. Chem. 99 (1995) 5117–5125, https://doi.org/10.1021/j100014a036.

[39] A. Auroux, J. Vedrine, Microcalorimetric characterization of acidity and basicity of various metallic oxides, Stud. Surf. Sci. Catal. Elsevier, 1985, pp. 311–318, https://doi.org/10.1016/S0167-2991(09)60180-4.

[40] H. Petitjean, K. Tarasov, F. Delbecq, P. Sautet, J.M. Krafft, P. Bazin, M.C. Paganini, E. Giamello, M. Che, H. Lauron-Pernot, Quantitative investigation of MgO Brønsted basicity: DFT, IR, and calorimetry study of methanol adsorption, J. Phys. Chem. C 114 (2010) 3008–3016, https://doi.org/10.1021/jp909354p.

[41] A. Gervasini, A. Auroux, Microcalorimetric investigation of the acidity and basicity of metal oxides, J. Therm. Anal. 37 (1991) 1737–1744, https://doi.org/10.1007/BF01912203.

[42] C. Pighini, T. Belin, J. Mijoin, P. Magnoux, G. Costentin, H. Lauron-Pernot, Microcalorimetric and thermodynamic studies of CO2 and methanol adsorption on magnesium oxide, Appl. Surf. Sci. 257 (2011) 6952–6962, https://doi.org/10.1016/j.apsusc.2011.03.040.

[43] J.C. Védrine, Acid–base characterization of heterogeneous catalysts: an up-to-date overview, Res. Chem. Intermed. 41 (2015) 9387–9423, https://doi.org/10.1007/s11164-015-1982-9.

[44] G. Busca, P.F. Rossi, V. Lorenzelli, M. Benaissa, J. Travert, J.C. Lavalley, Microcalorimetric and Fourier transform infrared spectroscopic studies of methanol adsorption on alumina, J. Phys. Chem. 89 (1985) 5433–5439, https://doi.org/10.1021/j100271a024.

[45] M.M. Branda, R.M. Ferullo, P.G. Belelli, N.J. Castellani, Methanol adsorption on magnesium oxide surface with defects: a DFT study, Surf. Sci. 527 (2003) 89–99, https://doi.org/10.1016/S0039-6028(03)00010-4.

[46] M. Bensitel, O. Saur, J.C. Lavalley, Use of methanol as a probe to study the adsorption sites of different MgO samples, Mater. Chem. Phys. 28 (1991) 309–320, https://doi.org/10.1016/0254-0584(91)90086-A.

[47] P.F. Rossi, G. Busca, V. Lorenzelli, Adsorption of methanol on alumina in the 298–473 K temperature range a microcalorimetric and FTIR spectroscopic study, Z. Phys. Chem. 149 (1986) 99–111, https://doi.org/10.1524/zpch.1986.149.1.099.